Indirect study of the stellar ^{34}Ar$(\alpha,p)^{37}$K reaction rate through ^{40}Ca$(p,t)^{38}$Ca reaction measurements

A. M. Long,[1,*] T. Adachi,[2] M. Beard,[1] G. P. A. Berg,[1] Z. Buthelezi,[3] J. Carter,[4] M. Couder,[1] R. J. deBoer,[1] R. W. Fearick,[5] S. V. Förtsch,[3] J. Görres,[1] J. P. Mira,[6] S. H. T. Murray,[3] R. Neveling,[3] P. Papka,[3,6] F. D. Smit,[3] E. Sideras-Haddad,[4] J. A. Swartz,[3,6,†] R. Talwar,[1,‡] I. T. Usman,[4] M. Wiescher,[1] J. J. Van Zyl,[6] and A. Volya[7]

[1]*Department of Physics and the Joint Institute for Nuclear Astrophysics, University of Notre Dame, Notre Dame, Indiana 46556, USA*
[2]*Research Center for Electron Photon Science, Tohoku University, Taihaku-ku, Sendai, Miyagi 982-0826, Japan*
[3]*iThemba Laboratory for Accelerator Sciences, Somerset West, Western Cape 7129, South Africa*
[4]*School of Physics, University Of Witwatersrand, Johannesburg, Gauteng 2050, South Africa*
[5]*Physics Department, University of Cape Town, Rondebosch, Western Cape 7700, South Africa*
[6]*Department of Physics, University of Stellenbosch, Matieland, Western Cape 7602, South Africa*
[7]*Department of Physics, Florida State University, Tallahassee, Florida 32306, USA*

(Received 24 February 2016; revised manuscript received 7 February 2017; published 10 May 2017)

The ^{34}Ar$(\alpha,p)^{37}$K reaction is believed to be one of the last in a sequence of (α,p) and (p,γ) reactions within the $T_z=-1$, sd-shell nuclei, known as the αp-process. This process is expected to influence the shape and rise times of luminosity curves coming from type I x-ray bursts (XRBs). With very little experimental information known on many of the reactions within the αp-process, stellar rates are calculated using a statistical model, such as Hauser-Feshbach. Questions on the applicability of a Hauser-Feshbach model for the ^{34}Ar$(\alpha,p)^{37}$K reaction arise due to level density considerations in the compound nucleus, ^{38}Ca. We have performed high energy-resolution forward-angle ^{40}Ca$(p,t)^{38}$Ca measurements with the $K=600$ spectrograph at iThemba LABS in order to identify levels above the α-threshold in ^{38}Ca. States identified in this work were then used to determine the ^{34}Ar$(\alpha,p)^{37}$K reaction rate based on a narrow-resonance formalism. Comparisons are made to two standard Hauser-Feshbach model predicted rates at XRB temperatures.

DOI: 10.1103/PhysRevC.95.055803

I. INTRODUCTION

Type I x-ray Bursts (XRBs) have been identified as thermonuclear runaways on the surface of accreting neutron stars within low mass x-ray binary (LMXB) systems [1–3]. As H/He rich material accretes onto the neutron star surface, it undergoes compression and heating until a thermonuclear runaway is triggered by a delicate interplay between the triple α reaction and α-induced breakout reactions on hot-CNO material [4,5]. Upon breaking out of the hot-CNO cycles, the thermonuclear runaway proceeds via the αp-process and the rp-process [6], riding along the proton drip line up to its possible endpoint around the Sn region [7]. Within the sd shell, the highly temperature dependent αp-process may dominate over the rp-process, depending on peak burst temperatures [8,9]. The main αp-reaction sequence starting from ^{18}Ne can be written as ^{18}Ne(α,p) ^{21}Na(p,γ) ^{22}Mg(α,p) ^{25}Al(p,γ) ^{26}Si(α,p) ^{29}P(p,γ) ^{30}S(α,p) ^{33}Cl(p,γ) ^{34}Ar(α,p) ^{37}K(p,γ) ^{38}Ca(α,p) ^{41}Sc$(p,\gamma)^{42}$Ti. Recent sensitivity studies have shown that some of these (α,p) reaction rates have a direct influence on the shape and rise times of luminosity curves observed during XRBs [10].

Over the past decade, much effort has gone into exploring the lower half of the αp-process through indirect studies of these (α,p) reactions, either using similar (p,t) measurements [11–14] or time-inverse reactions with radioactive beams [15]. Unfortunately very little experimental information exists on (α,p) reactions at higher masses in the αp-process, near the closed shell $N,Z=20$. In the absence of experimental information on a particular (α,p) reaction, its rate is predicted using a statistical model, such as Hauser-Feshbach (HF) [16]. In order to reliably utilize a HF model prediction for a specific astrophysical reaction, there must be a sufficiently high level density at the relevant astrophysical energies within the compound nucleus. Past studies on the applicability of a HF model for thermonuclear rates have pointed out that for a HF predicted rate to be considered reliable (within 20% accuracy), at least 10 non-overlapping narrow resonances must lie within the effective astrophysical energy window [17]. The relatively low α-threshold in ^{38}Ca, 6105.12(21) keV [18], and the fact that only natural parity states above this threshold will participate as resonances in the ^{34}Ar(α,p) reaction suggest that the statistical approach used by a HF model might not be valid for this reaction at XRB temperatures. Instead, this rate may depend critically on the number and characteristics of resonances within the relevant astrophysical energies. For temperatures observed in XRBs, starting from roughly $T\sim 0.7$ GK and extending up to $T\sim 2.0$ GK, the relevant energy range where levels in ^{38}Ca will be most influential as resonances in the ^{34}Ar(α,p) reaction can be calculated using the Gamow window approximation [19], and roughly corresponds to 7–10 MeV in excitation energy.

*Current address: Physics Division, Los Alamos National Laboratory, Los Alamos, New Mexico 87545, USA; alexlong@lanl.gov.
†Current address: KU Leuven, Instituut voor Kern- en Stralingsfysica, Celestijnenlaan 200D, 3001 Leuven, Belgium.
‡Current address: Physics Division, Argonne National Laboratory, Argonne, Illinois 60439, USA.

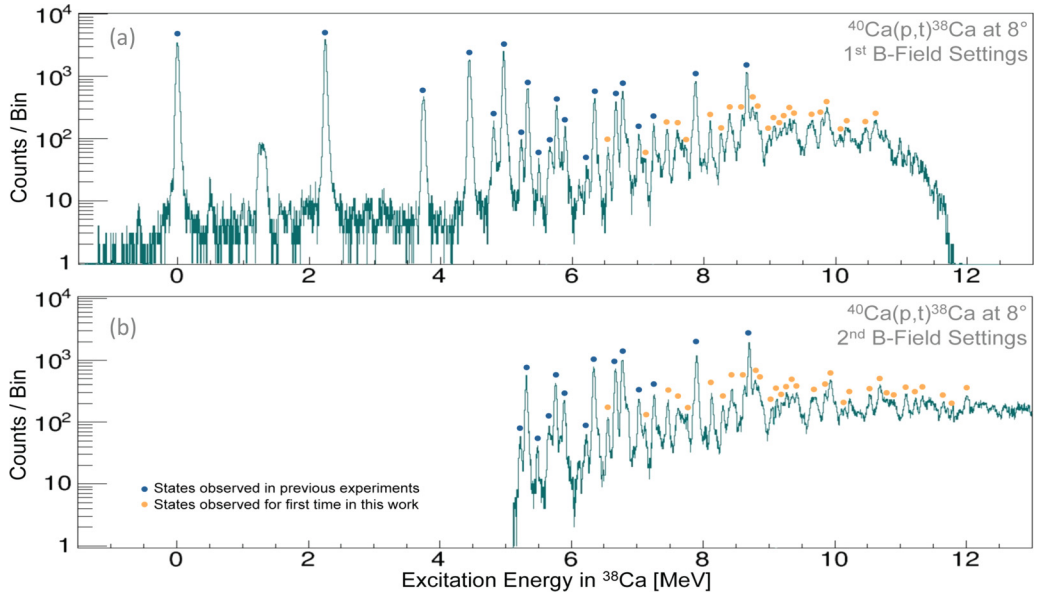

FIG. 1. ^{38}Ca spectra in the focal plane of the $K = 600$ spectrograph shown at $\theta_{lab} = 8^\circ$ with two different field settings [panels (a) and (b)] to cover a full energy region from the ground state to 13 MeV in excitation energy in ^{38}Ca. The spectra shown here have been background subtracted using two particle identification gates, namely energy loss and time of flight. Peaks with dark dots (blue online) are states that have been observed in previous experiments investigating ^{38}Ca, while peaks with lighter dots (orange online) represent states observed for the first time in this work.

Currently, there are only a handful of known states above the α-threshold in ^{38}Ca from previous (p,t) and $(^3\text{He},n)$ experiments [20–22]. With this in mind, we have performed an indirect study of the $^{34}\text{Ar}(\alpha,p)^{37}\text{K}$ reaction by investigating the level structure above the α-threshold in ^{38}Ca using high energy-resolution zero-degree $^{40}\text{Ca}(p,t)^{38}\text{Ca}$ reaction measurements.

In this paper we present the level structure of α-unbound states within ^{38}Ca as populated by the $^{40}\text{Ca}(p,t)^{38}\text{Ca}$ reaction using the $K = 600$ magnetic spectrograph at iThemba LABS, with the main goal of identifying possible resonances in the $^{34}\text{Ar}(\alpha,p)^{37}\text{K}$ reaction at XRB temperatures. The techniques and experimental setup for this work are reviewed in Sec. II, while the results of identified levels in ^{38}Ca are discussed in Sec. III along with comparisons to previous works. In Sec. IV we use the level structure information observed in this work to derive an $^{34}\text{Ar}(\alpha,p)^{37}\text{K}$ reaction rate and compare it to standard HF rates used in XRB models.

II. EXPERIMENTAL TECHNIQUES

The experimental techniques of high energy-resolution forward-angle (p,t) measurements with magnetic spectrographs to investigate possible (α,p) resonances in $T_z = (N-Z)/2 = -1$ sd-shell nuclei have been well developed at the Research Center for Nuclear Physics (RCNP) with the Grand Raiden (GR) spectrograph and at iThemba LABS with the $K = 600$ spectrograph. These experimental techniques are discussed in detail in previous works [11,13,14,23], and therefore only summarized here.

A. Experimental setup

For this experiment, a 100-MeV proton beam was produced and delivered by the $K = 200$ Separated Sector Cyclotron (SSC) of iThemba LABS, through the X, P1, P2, and S beam lines, to the target chamber positioned in front of the $K = 600$ spectrograph, where it impinged upon a 2.1 mg/cm^2, highly enriched ($\geqslant$99%), self-supporting ^{40}Ca target. The reaction products, along with the beam, were then momentum analyzed using the $K = 600$ spectrograph. The beam was collected in the beam stop located inside dipole D1 of the spectrograph, while tritons were transported to the focal plane detector system. The focal plane detector system consisted of XU-wire drift chambers, yielding horizontal and vertical position and angle, and two plastic scintillating detectors for particle identification through ΔE and time-of-flight information [23]. Dispersion matching techniques, as described in Refs. [24,25], were used to achieve high energy resolution ($\sim$35 keV) in the focal plane, which is dominated by energy loss and straggling through the target. Background contaminations coming from reactions such as $^{12}\text{C}(p,t)$ and $^{16}\text{O}(p,t)$ were identified using a 2.1 mg/cm^2 mylar target.

While the main focus of this experiment was to identify states in the excitation energy range above the α-threshold relevant for XRBs ($\sim$7–10 MeV), a full range of excitation energies from the ground state to 13 MeV was investigated. Due to the $K = 600$ spectrograph's momentum acceptance of 10%, an overlapping technique with two different field settings was used to cover the full 13 MeV excitation energy region [11], as seen in Fig. 1. Furthermore, to aid in the identification of states from ^{38}Ca, measurements at two angles ($\theta_{lab} = -1.2^\circ$ and 8°) were performed.

TABLE I. States identified below the α-threshold, along with previous (p,t) and $(^3\text{He},n)$ experiments populating states in ^{38}Ca. Proton and α-thresholds are located at 4547.27(22) keV and 6105.12(21) keV in excitation energy, respectively. All excitation energies are given in keV.

This work	Paddock *et al.* [20]		Kubono *et al.* [21]		Alford *et al.* [22]	
^{40}Ca$(p,t)^{38}$Ca	^{40}Ca$(p,t)^{38}$Ca	J^π	^{40}Ca$(p,t)^{38}$Ca	J^π	^{36}Ar$(^3\text{He},n)^{38}$Ca	J^π
g.s.[a]	g.s.	0^+	g.s.	0^+	g.s.	0^+
2214.8(32)[a]	2206(5)	2^+	2200(30)	2^+	2250(70)	(2)
			3060(30)	0^+	3070(30)	
3695.2(44)	3695(5)		3690(30)	2^+	3670(30)	(2)
			3720(30)			
	4191(5)		4180(30)	(5^-)		
4387.1(35)[a]	4381(5)	(2^+)	4370(30)	2^+	4390(30)	2^+
4753.8(63)	4748(5)		4750(30)	3^-		
4903.5(34)[a]	4899(5)	(2^+)	4890(30)	2^+	4860(40)	(3)
5170(8)	5159(7)				5140(60)	
5267(4)	5264(5)		5250(30)	2^+		
5438(9)	5427(6)					
5608(10)	5598(7)		5600(30)		5560(60)	(3)
5705(5)	5698(10)					
5832(8)	5810(5)		5810(30)		5790(40)	(4)

[a]States in ^{38}Ca used to match spectra at each angle to absolute calibration.

B. Reference data and focal plane calibration

To accurately identify α-unbound levels in ^{38}Ca, the calibration of the focal plane must be achieved with great care. The method used to calibrate the focal plane of the $K = 600$ spectrograph follows the same procedures taken from previous high energy-resolution (p,t) experiments performed at RCNP with the Grand Raiden spectrograph [11,13]. An absolute calibration of the focal plane was performed using the ^{24}Mg$(p,t)^{22}$Mg reaction, where the ground state, along with 7 strongly populated natural parity states up to 6.226 MeV, fully covered the focal plane. With most magnetic spectrographs, the position in the focal plane has a linear relationship to the particle's momentum in first order, while a quadratic term is introduced to account for higher orders. Along with an absolute calibration of the focal plane, spectra at both angles were matched and calibrated using the well known 0^+ and 2^+ states below the α-threshold in ^{38}Ca (see Table I).

All peaks identified in the focal plane spectra were fitted with a symmetric Gaussian distribution and the position of the peak was then determined by the centroid. Isolated peaks were fitted with a single Gaussian distribution, while groups of closely spaced peaks were fitted with multiple Gaussian distribution simultaneously.

Final uncertainties in all identified levels are given by a combination of systematic and statistical errors, added quadratically. Systematic uncertainties include that of the energy calibration, reaction angle determination ($\pm 0.1^\circ$), target thickness (± 0.21 mg/cm^2), and the reaction Q-value of ^{40}Ca$(p,t)^{38}$Ca (0.2 keV from [18]), or in other words the uncertainty in the masses of the nuclei involved. The statistical uncertainty is given as the full width at half maximum (FWHM) divided by the area of the Gaussian fit for each identified peak.

III. EXPERIMENTAL RESULTS

In this experiment, a total of 45 states were identified in ^{38}Ca, 4 states below the proton threshold, 4547.27(22) keV [18], 8 states between the proton and α-threshold, 6105.12(21) keV [18], and 33 states above the α-threshold up to 12 MeV in excitation energy. Of the 45 states, a total of 25 were observed for the first time in this work. States were identified only if they were confirmed at both angles, with the exception of 9 states that showed strong signals in the $\theta_{\text{lab}} = 8^\circ$ spectra but were covered by background in the $\theta_{\text{lab}} = -1.2^\circ$ spectra.

A. States below the α-threshold

Prior to this work, three experiments probed excited states in ^{38}Ca [20–22]. States identified in this work below the α-threshold from the ^{40}Ca$(p,t)^{38}$Ca reaction are given in Table I, along with previous measurements. The well-known ground state (g.s.), 2214.8 keV, 4387.1 keV, and 4903.5 keV states were all used to match the absolute calibration to the ^{38}Ca spectra at both angles. Of the states below the α-threshold reported here, most agree well with previous works with the exception of the 5832(8) keV state that is slightly higher than the values of 5810(5) keV and 5790(40) keV previously reported by Paddock *et al.* [20] and Alford *et al.* [22], respectively.

B. States above the α-threshold

These α-unbound states in ^{38}Ca identified in this work are expected to contribute as natural parity resonances to the cross section of ^{34}Ar$(\alpha,p)^{37}$K. Prior to this work only 8 states were experimentally known above the α-threshold of 6105.12(21) keV. In total, 33 states above the α-threshold

TABLE II. Observed α-unbound states in this work, along with previous (p,t) [20,21] and (^{3}He,n) [22] experiments identifying α-unbound states in ^{38}Ca. All excitation energies are given in keV. Peaks followed by asterisks * were only identified in the $\theta_{lab} = 8^\circ$ spectrum.

Present ^{40}Ca(p,t)	Ref. [20] ^{40}Ca(p,t)	Ref. [21] ^{40}Ca(p,t)	Ref. [22] ^{36}Ar(^{3}He,n)
6277(3)	6280(8)	6270(30)	
6485(6)			
6601(3)	6598(7)	6600(30)	
6704(3)	6702(10)		6760(50)
6772(13)	6801(12)		
6950(5)			
7041(8)			
7176(4)			7200(50)
7370(5)			
7480(9)			7470(50)
7801(3)	7800(12)	7800(30)	
8026(5)			
8189(6)			
8322(5)			
8507(9)			
8586(3)	8595(10)		
8672(6)			
8717(8)*			
8924(9)*			
8994(9)*			
9073(9)			
9157(8)			
9230(9)*			
9296(8)*			
9735(8)			
9809(6)			
10104(9)			
10410(9)			
10557(8)			
10946(11)*			
11089(11)*			
11189(13)*			
11861(11)*			

up to ∼12 MeV were observed in this work, of which 25 states are reported for the first time. All states identified in this work, along with previous (p,t) and (^{3}He,n) measurements are reported in Table II. It should be noted that 9 states were strongly identified at $\theta_{lab} = 8^\circ$, but could not be confidently identified at $\theta_{lab} = -1.2^\circ$ due to high background from secondary scattering of the beam on the beam stop inside dipole D1. These 9 states (displayed with an asterisk * in Table II) were included in the final results because they displayed the same kinematic shift over the horizontal angle acceptance of the $K = 600$ spectrograph at $\theta_{lab} = 8^\circ$ ($\pm 2.5^\circ$) as observed for other ^{38}Ca states, and thus clearly represents a state in ^{38}Ca and cannot be considered to be a contaminant peak.

IV. THE ^{34}Ar$(\alpha,p)^{37}$K REACTION RATE

The ^{34}Ar nucleus is believed to play an important role in the αp-process. Due to a relatively long β-decay half-life of 843.8(4) ms [26], and a low Q-value for the ^{34}Ar(p,γ) reaction, $Q_{(p,\gamma)} = 140.96$ keV, ^{34}Ar is considered a possible waiting point within the rp-process. The ^{34}Ar$(\alpha,p)^{37}$K reaction within the αp-process may act as a bypass for this waiting point depending on its reaction strength. Currently this reaction rate is based on HF model predictions with no experimental constraints. In this work we have identified 33 states above the α-threshold that could act as resonances within the ^{34}Ar$(\alpha,p)^{37}$K reaction. For this calculation, we assume all observed states in this work are of natural parity, and therefore will participate in the ^{34}Ar$(\alpha,p)^{37}$K reaction. This natural parity assumption stems from the mechanism through which these states are populated. At high incoming proton energies (100 MeV in this work), the (p,t) reaction is thought to be dominated by a one-step two-particle spin-zero transfer process [27]. This direct process offers a selectivity of predominately populating natural parity states in the recoil nucleus of ^{38}Ca, when observed at very forward scattering angles. With this assumption, the stellar ^{34}Ar$(\alpha,p)^{37}$K reaction rate can be explored based on the results of this work.

A. Narrow-resonance reaction rate formalism

For the majority of resonances within the relevant energy range, the total resonance width, which is the sum of all open channel partial widths ($\Gamma_{tot} = \Gamma_\alpha + \Gamma_p + \Gamma_\gamma$), will be dominated by the proton partial width, Γ_p. Within this energy region, α partial widths (Γ_α) will be considerably smaller than the proton partial widths due to a lower Coulomb penetrability for low energy α's. Additionally, γ strengths (Γ_γ) for even the most probably transitions within this energy region can be considered at most on the order of eV, and therefore much smaller than the corresponding proton-partial width. With these considerations, the total resonances width can be approximated as just the proton partial width, $\Gamma_{tot} \simeq \Gamma_p$. Using these widths, it can be shown that conditions within this energy region are such that a narrow-resonance formalism can be adopted to determine the total reaction rate. Here, the condition for a narrow resonance is taken quantitatively as $\Gamma_{tot}/E_{res} \leqslant 10\%$ [28], where, E_{res} is the center-of-mass energy of the resonance.

The possibility of narrow resonance conditions in ^{38}Ca is illustrated in Fig. 2, where proton single-particle widths, Γ_p^{sp}, for the ^{37}K + p system are plotted as a function of proton center-of-mass energy given a range of orbital angular momenta, $\ell = 0$–4. Current shell model calculations, using modern available interaction Hamiltonians of [29–31], demonstrate that proton spectroscopic factors (C^2S_p) for levels within the relevant energy region in ^{38}Ca ($E_x \approx 7$–10 MeV) fall with a range of $C^2S_p = 0.1$–0.01. Taking this range of proton spectroscopic factors, and calculating proton partial widths as $\Gamma_p = C^2S_p\Gamma_p^{sp}$, it can be seen from Fig. 2 that within the relevant region, proton partial widths, and therefore total widths, are small enough for the resonances to be considered narrow ($\Gamma_{tot} \leqslant 10\%\ E_{res}$).

Given the above interpretation that the resonance within this energy region meet the conditions of narrow resonances, a narrow-resonance formalism (as outlined in Ref. [19]) is adopted to calculate the total ^{34}Ar$(\alpha,p)^{37}$K reaction rate.

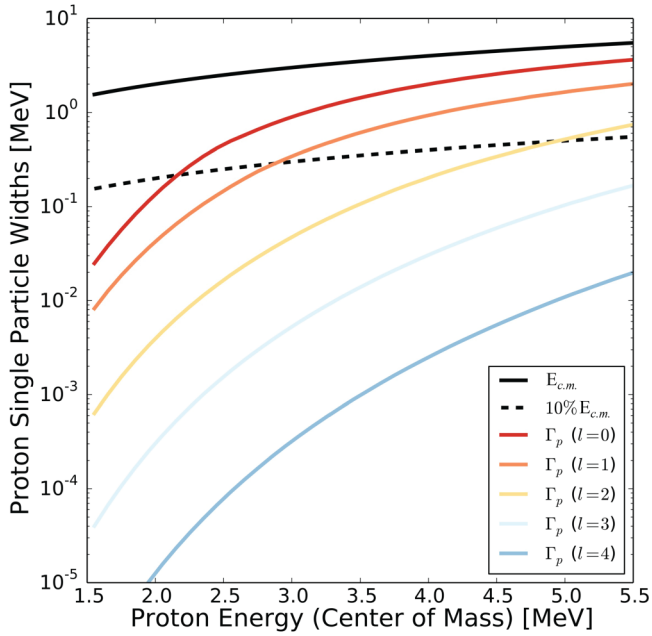

FIG. 2. Calculated proton particle-widths as a function of center-of-mass energy given a range of orbital angular momenta, $\ell = 0$–4. A proton center-of-mass energy range of 1.5–5.5 MeV approximately corresponds to an excitation energy range of 6–10 MeV in ^{38}Ca.

Within this formalism, the total reaction rate can be expressed as a sum of the reaction rate over individual resonances i:

$$N_A\langle\sigma v\rangle = 1.54 \times 10^{11}(\mu T_9)^{-3/2} \times \sum_i (\omega\gamma)_i \exp\left(\frac{-11.605E_i}{T_9}\right), \quad (1)$$

with μ being the reduced mass (amu), T_9 the temperature (10^9 K), $(\omega\gamma)$ the resonance strength (MeV), and E_i the resonance energy in the center-of-mass system (MeV). The resonance strength is defined as

$$(\omega\gamma)_i = \frac{2J_i + 1}{(2j_1 + 1)(2j_2 + 1)}\frac{\Gamma_a\Gamma_b}{\Gamma_{\text{tot}}}. \quad (2)$$

J_i, j_1, and j_2 are the spins of the level, projectile, and target, respectively. Here, Γ_a and Γ_b are the partial widths for the formation and decay of the compound nucleus, respectively, and Γ_{tot} is the total width of the state. In the case of the ^{34}Ar$(\alpha, p)^{37}$K reaction, J_i, $j_1 = j_\alpha = 0$, and $j_2 = j_{(^{34}\text{Ar})} = 0$ are the total angular momenta of the level, the α particle, and ^{34}Ar, respectively. For the partial widths, $\Gamma_a = \Gamma_\alpha$ and $\Gamma_b = \Gamma_p$, with the total width being $\Gamma_{\text{tot}} = \Gamma_\alpha + \Gamma_p + \Gamma_\gamma$. As discussed previously, the total widths will be dominated by the proton partial widths ($\Gamma_p \gg \Gamma_\alpha$ and Γ_γ, therefore $\Gamma_{\text{tot}} \simeq \Gamma_p$). With this approximation, Eq. (2) simplifies to

$$(\omega\gamma)_i \approx (2J_i + 1)\Gamma_\alpha. \quad (3)$$

The α partial width can be given as

$$\Gamma_\alpha = C^2S_\alpha\Gamma_\alpha^{sp} \quad (4)$$

where C^2S_α is the α spectroscopic factor and Γ_α^{sp} is the α single-particle width.

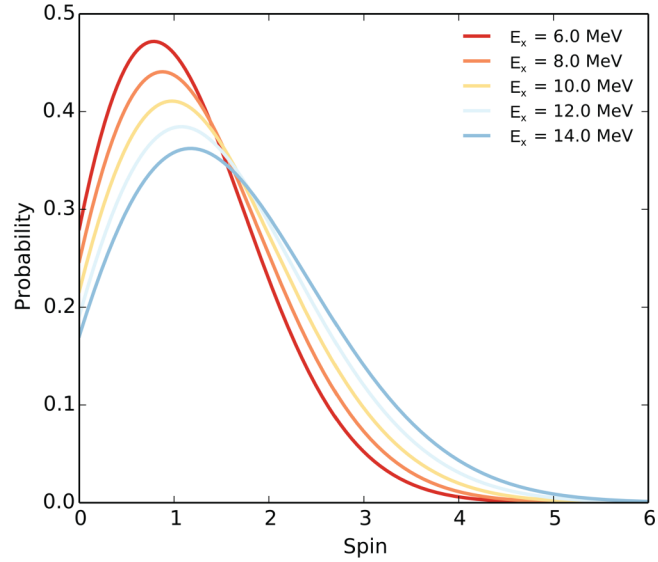

FIG. 3. Spin distributions for selected excitation energies in ^{38}Ca based on Eq. (5) used in the framework of the BSFG model.

Currently, no experimental information exists on spins, or α-spectroscopic factors, for states above the α-threshold in ^{38}Ca. In order to extract a ^{34}Ar$(\alpha, p)^{37}$K reaction rate using Eq. (1), given that only resonance energies are known from this work, additional information on spins and α-spectroscopic factors must be derived using various models.

B. Treatment of unknown spins and α-spectroscopic factors

Given the lack of experimental information on spins for α-unbound states in ^{38}Ca, a random sampling procedure from spin distributions derived using the backshifted Fermi gas (BSFG) model [32] was implemented for spin assignments. Within this model, spin distributions, as a function of excitation energy, can be written as

$$R(E_x, J) = \frac{2J + 1}{2\sigma^2}\exp\left[-\frac{(J + 1/2)^2}{2\sigma^2}\right]. \quad (5)$$

Here, E_x is the excitation energy in ^{38}Ca, J is the level spin, and σ is the spin cut-off parameter, which is a function of excitation energy, $\sigma(E_x)$. For this calculation, the spin cut-off parameter function was taken directly from the parameters given in TALYS 1.8 [33]. For further review of this spin distribution function and the parameters used; see Sec. 4.7 in the TALYS-1.8 User Manual [34]). Within the excitation energy range of interest, these spin distributions (as illustrated in Fig. 3) favor lower spins and peak roughly around $J = 1$.

In addition to unknown spins, no experimental information exists concerning α-spectroscopic factors (α-SFs) for α-unbound states in ^{38}Ca. Given that these α-SF values will directly impact the reaction rate through the resonance strengths of each state, the assumptions made in determining this missing information becomes critical in the resultant ^{34}Ar$(\alpha, p)^{37}$K reaction rate calculation. With this in mind, two sets of α-SF values are determined with the intent to represent

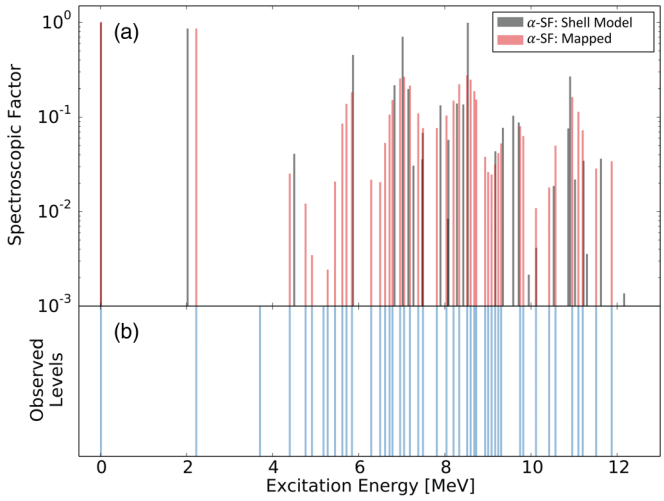

FIG. 4. (a) α-spectroscopic factors for states in ^{38}Ca calculated using the shell model as described in Ref. [39] (shown in gray), along with the mapped values to states observed in this work (overlaid). (b) Level density of observed states in ^{38}Ca from this work along with previous works.

two distinct possibilities: the existence or nonexistence of α-cluster states.

Previous α-transfer and knock-out studies within the *sd* shell have shown that ground state α-spectroscopic strengths increase around the shell closer $N, Z = 8$ and $N, Z = 20$ [35–37]. Additionally, an extensive study of clustering in ^{40}Ca by Yamaya *et. al.* [38] unveiled significant α-clustering structure in various excited states ranging up to 15 MeV in excitation energy.

To represent the possibility of cluster states above the α-threshold in ^{38}Ca, α-SFs are calculated using a cluster-nucleon configuration interaction mode [39] that extends the traditional shell model approach. In this calculation, shell model Hamiltonians from [30] are utilized while states with up to two particle-hole excitations are taken into account. For further review see [39] and references therein.

The resultant α-SFs from this shell model calculation are illustrated in Fig. 4 (shown in gray). Examining Fig. 4, it can be seen that this type of shell model calculation predicts a hierarchy of states based on their α-SF values, where a few strong α-cluster states above the α-threshold will dominate the total ^{34}Ar$(\alpha, p)^{37}$K reaction rate.

Given that the excitation energies of states from the shell model calculations do not exactly match up with the observed states, α-SF values are mapped onto the observed states in this work using Gaussian smoothing functions.

For this procedure, each observed state is smeared using a Gaussian function with some energy width, σ, which can be written as

$$G(E) = \frac{1}{\sigma\sqrt{2\pi}}\, e^{-\frac{1}{2}(E/\sigma)^2}. \tag{6}$$

For this calculation, a smearing width of $\sigma = 150$ keV is taken for all states. Summing over all observed states in this work, an observed level density function can be taken as

$$\rho^{\text{obs}}(E_{ex}) = \sum_{\mu} G\left(E_{ex} - E_{\mu}^{\text{obs}}\right), \tag{7}$$

where, E_{μ}^{obs} are the excitation energies of individual levels observed in this work. Using the observed level density function of Eq. (7), α-SFs for observed states can be derived based on the predicted set of α-SF values,

$$S_{\mu}^{\text{obs}} = \sum_{\nu} \frac{S_{\nu}^{sm}}{\rho^{\text{obs}}(E_{\nu})}\, G\left(E_{\mu}^{\text{obs}} - E_{\nu}^{sm}\right), \tag{8}$$

where S_{ν}^{sm} and E_{ν}^{sm} are the shell model predicted α-SFs and excitation energies of individual levels, respectively. Here, the normalization of shell model predicted states by local density of observed states assures preservation of the sum rule over the shell model predicted α-SFs,

$$\begin{aligned}\sum_{\mu} S_{\mu}^{\text{obs}} &= \sum_{\nu} \frac{S_{\nu}}{\rho^{\text{obs}}\left(E_{\nu}^{sm}\right)} \sum_{\mu} G\left(E_{\mu}^{\text{obs}} - E_{\nu}^{sm}\right) \\ &= \sum_{\nu} S_{\nu}^{sm}\end{aligned} \tag{9}$$

The results of this Gaussian smearing procedure in assigning α-SF values to experimental states, given a smearing width of $\sigma = 150$ keV, is illustrated in Fig. 4 (shown in red). The mapped α-SF values based on these shell model calculations are then used to determine the ^{34}Ar$(\alpha, p)^{37}$K reaction rate, given the possibly of strong α-clustering above the α-threshold.

In the case of non-α-cluster states, a global α-spectroscopic factor of $S_{\alpha} = 0.01$ is adopted, meaning that all α partial widths (Γ_{α}) are about 1% of the total single-particle widths (Γ_{α}^{sp}). This approach of using a relatively small α-SF value globally follows previous works performing similar (α, p) reaction calculations within the *sd* shell [13,14]. This global SF value was chosen not only for comparison with other previous (α, p) rate studies, but also to illustrate the the influence α-cluster states, vs non-α-cluster states, in ^{38}Ca would have on the ^{34}Ar$(\alpha, p)^{37}$K rate. Given these two sets of α-SF values, two total reaction rate calculations were performed using Eq. (1).

C. Calculating the total rate

With the information from levels observed in this experiment, along with the assumptions of spins and α-spectroscopic factors described in Sec. IV B, a Monte Carlo–like calculation was performed based on Eq. (1) for a given range of stellar temperatures observed in XRB environments. To begin, each state is assigned a spin by randomly sampling from spin distributions generated by Eq. (5) using the rejection-acceptance method [40].

Given a particular spin assignment set, α-single-particle widths are calculated for each state using the BIND subroutine in the DWUCK4 code [41], which calculates single-particle radial wave functions based on the solution to the Schrödinger equation with a real potential and a given set of quantum numbers (for further review see the Appendix of [42]). It should be noted that each set of quantum numbers needed for a particular α single-particle radial wave function (based

on the orbital angular momentum of the α particle) was determined using the the Wildermuth condition (see [43] and references therein). Once single-particle widths are calculated, α partial widths are determined using Eq. (4), along with the corresponding α-SF values. With this given set of spins and α partial widths, resonances strengths are determined using Eq. (2) for all states, and Eq. (1) is then used to calculate the total reaction rate as a function of temperature.

This total rate calculation was repeated $N = 10^7$ times with different spin-set combinations, producing a distribution of rates at a given temperature for a range of temperatures relevant to XRBs. At each temperature, a median rate is determined by calculating the 0.50 quantile of the rate distribution. Finally, this median rate is taken as the ^{34}Ar$(\alpha, p)^{37}$K total reaction rate, and plotted as a function of temperature (shown in Fig. 5).

As mentioned in Sec. IV B, this total rate calculation is performed twice for the two different sets of α-SFs, once with the mapped shell model α-SF values, meant to represent the possibility of α-cluster states in ^{38}Ca (labeled as median rate 2), and another with global α-SF values of $S_\alpha = 0.01$, meant to represent the possibility of no α-clustering in ^{38}Ca (labeled as median rate 1).

For comparison with HF predictions, the two median rates are plotted alongside two HF model predicted rates from NON-SMOKER$^{\text{WEB}}$ v5.0w [44] and TALYS 1.8 [33]. Additionally, both median rates from this work, along with the two HF model predictions, are listed in Table. III for further comparison at, and slightly beyond, typical XRB temperatures. The temperature range relevant to XRB light curves starts at $T \sim 0.7$ GK and extends up to peak burst temperatures of $T \sim 2.0$ GK. As seen in Fig. 5, throughout this temperature range, both median rates from this work are lower than the HF predictions of NON-SMOKER$^{\text{WEB}}$ v5.0w and TALYS 1.8, though median rate 1 is significantly lower. The lower values of the median 1 rate suggest that level density in ^{38}Ca, based on the number of levels observed in this work, is not high enough to meet the criterion needed to reliably apply the statistical model to predict the ^{34}Ar$(\alpha, p)^{37}$K cross section, and subsequent reaction rate, at the relevant astrophysical energies observed in XRBs. Instead, this suggests that this reaction is most likely governed by a handful of resonances corresponding to levels located within the relevant excitation energy range in ^{38}Ca.

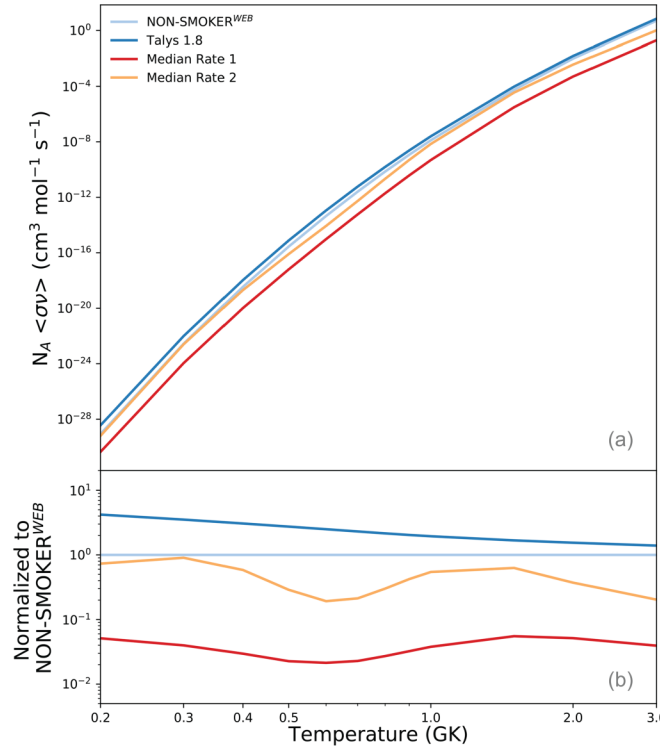

FIG. 5. (a) ^{34}Ar$(\alpha, p)^{37}$K reaction rates as a function of stellar temperature for statistical model predictions, NON-SMOKER$^{\text{WEB}}$ v5.0w and TALYS 1.8, along with the two median rates calculated in this work, median rate 1 (without α-clustering) and median rate 2 (with α-clustering). (b) All rates are normalized to the NON-SMOKER rate.

TABLE III. The total reaction rate $N_A\langle\sigma v\rangle$, in units of cm^3 mole^{-1} s^{-1}, as a function of temperature from the narrow-resonance calculation based on this work. Listed are the resultant median rates from this work, meant to account for the possibilities of α-clustering and non-α-clustering, along with two standard HF model predictions from NON-SMOKER$^{\text{WEB}}$ v5.0w and TALYS 1.8 for comparison.

Temperature (GK)	NON-SMOKER$^{\text{WEB}}$	TALYS 1.8	Median rate 1	Median rate 2
0.10	2.99×10^{-43}	6.21×10^{-43}	1.71×10^{-44}	5.69×10^{-44}
0.15	5.39×10^{-35}	2.48×10^{-34}	3.81×10^{-36}	3.89×10^{-35}
0.20	8.59×10^{-30}	3.62×10^{-29}	4.40×10^{-31}	6.30×10^{-30}
0.30	2.79×10^{-23}	9.83×10^{-23}	1.11×10^{-24}	2.52×10^{-23}
0.40	3.48×10^{-19}	1.07×10^{-18}	1.03×10^{-20}	2.04×10^{-19}
0.50	2.79×10^{-16}	7.64×10^{-16}	6.31×10^{-18}	8.04×10^{-17}
0.60	4.49×10^{-14}	1.12×10^{-13}	9.59×10^{-16}	8.64×10^{-15}
0.70	2.56×10^{-12}	5.91×10^{-12}	5.84×10^{-14}	5.45×10^{-13}
0.80	7.11×10^{-11}	1.53×10^{-10}	1.93×10^{-12}	2.14×10^{-11}
0.90	1.17×10^{-09}	2.38×10^{-09}	3.77×10^{-11}	4.93×10^{-10}
1.00	1.29×10^{-08}	2.51×10^{-08}	4.87×10^{-10}	7.01×10^{-09}
1.50	5.60×10^{-05}	9.40×10^{-05}	3.09×10^{-06}	3.52×10^{-05}
2.00	9.80×10^{-03}	1.51×10^{-02}	5.04×10^{-04}	3.64×10^{-03}
2.50	3.54×10^{-01}	5.17×10^{-01}	1.56×10^{-02}	8.64×10^{-02}
3.00	$5.10 \times 10^{+00}$	$7.10 \times 10^{+00}$	2.00×10^{-01}	$1.04 \times 10^{+00}$

Furthermore, the shape of median rate 2, along with its large discrepancy with median rate 1 within certain temperatures ranges, illustrates the influence of possible α-cluster states on the total reaction rate. Here, median rate 2 (taken using the shell model α-SF value) is much closer to HF predictions within certain temperature ranges not because there are many, many states contributing in a statistical manor, but because there are one or two α-cluster-like states within the relevant energy range dominating the total reaction rate at these particular temperatures. The discrepancies between the two median rates, along with the overall shape of median rate 2, emphasis the need to further study the α-strength structure of α-unbound states in ^{38}Ca. Depending on which states exhibit α-clustering, the total $^{34}\mathrm{Ar}(\alpha,p)^{37}\mathrm{K}$ reaction rate will be enhanced within the corresponding temperature ranges, as seen with median rate 2 in Fig. 5.

V. CONCLUSIONS

We have presented experimental measurements of states above the α-threshold in ^{38}Ca up to $E_x \sim 12$ MeV. With precise energy information on possible resonances taken from this work, combined with model assumptions to fill in the missing information on spins and α-spectroscopic factors, distributions of the total $^{34}\mathrm{Ar}(\alpha,p)^{37}\mathrm{K}$ reaction rate across XRB temperatures were generated using a Monte Carlo–like approach (varying only spin values) within a narrow-resonance reaction rate formalism. A median rate, taken as the 50% quantile from each distribution, is then quoted as the total $^{34}\mathrm{Ar}(\alpha,p)^{37}\mathrm{K}$ rate as a function of temperature. Additionally, possible effects of α-clustering within the α-unbound states in ^{38}Ca on the total rate are initially explored using two different sets of α-spectroscopic factor values within a narrow-resonance reaction rate calculation. Both median rates are compared to predicted rates determined using statistical HF models, specifically NON-SMOKER$^{\mathrm{WEB}}$ v5.0w and TALYS 1.8. Comparing the non-α-cluster rate to HF predictions suggests that a statistical HF approach may not be suitable for the $^{34}\mathrm{Ar}(\alpha,p)^{37}\mathrm{K}$ reaction rate at XRB temperatures as there may be an insufficient number of levels in ^{38}Ca at the appropriate bombarding energies. Instead, this reaction is most likely governed by a handful of resonances located within the relevant energy window for most temperatures observed in XRBs. Furthermore, comparing median rate 1 to median rate 2 highlights the impact possible α-clustering in ^{38}Ca would have on the total $^{34}\mathrm{Ar}(\alpha,p)^{37}\mathrm{K}$ rate.

It should be noted that the two total $^{34}\mathrm{Ar}(\alpha,p)^{37}\mathrm{K}$ reaction rates quoted in this work (Table III) are strongly dependent on the assumptions made in determining the missing information to obtain the rate. Specifically, we assume that all states in this work contribute to the total reaction, that the states are isolated enough to use of a narrow-resonance formalism, and we use specific models to obtain spin and α-SF values. In this sense, the derived $^{34}\mathrm{Ar}(\alpha,p)^{37}\mathrm{K}$ reaction rates from this work, given the above described assumptions, should solely be taken as exploratory, first in comparisons with statistical models, and second in investigating the effects of possible α-cluster states above the α-threshold. This work is just the first step in experimentally determining the $^{34}\mathrm{Ar}(\alpha,p)^{37}\mathrm{K}$ reaction rate at XRB temperatures. With 33 states in ^{38}Ca now identified as possible resonances in the $^{34}\mathrm{Ar}(\alpha,p)^{37}\mathrm{K}$ reaction, future experiments should focus on either searching for additional states in ^{38}Ca missed in this work that may act as resonances, or determining much-needed spin and α-spectroscopic information on α-unbound states observed in this work.

ACKNOWLEDGMENTS

The authors are grateful for the help and support of the technical staff at iThemba LABS during the course of the experiment PR137. This work was supported by the National Science Foundation through Grant No. PHY-1068192 and The Joint Institute for Nuclear Astrophysics Center for the Evolution of the Elements through Grants No. PHY-0822648 and No. PHY-1430152, along with the financial assistance of the South African National Research Foundation. Additionally, this material is based upon work supported by the US Department of Energy, Office of Science, Office of Nuclear Physics under Grant No. DE-SC0009883.

[1] S. E. Woosley and R. E. Taam, Nature (London) **263**, 101 (1976).
[2] P. C. Joss, Nature (London) **270**, 310 (1977).
[3] D. Q. Lamb and F. K. Lamb, Astrophys. J. **220**, 291 (1978).
[4] J. Fisker, W. Tan, J. Görres, M. Wiescher, and R. L. Cooper, Astrophys. J. **665**, 637 (2007).
[5] L. Keek, R. H. Cyburt, and A. Heger, Astrophys. J. **787**, 101 (2014).
[6] R. K. Wallace and S. E. Woosley, Astrophys. J. Suppl. Ser. **45**, 389 (1981).
[7] H. Schatz, A. Aprahamian, V. Barnard, L. Bildsten, A. Cumming, M. Ouellette, T. Rauscher, F. K. Thielemann, and M. Wiescher, Phys. Rev. Lett. **86**, 3471 (2001).
[8] L. Van Wormer, J. Görres, C. Iliadis, M. Wiescher, and F.-K. Thielemann, Astrophys. J. **432**, 326 (1994).
[9] H. Schatz, A. Bacher, G. P. A. Berg, T. Black, S. Choi, C. Foster, J. Görres, K. Jiang, B. Lozowski, E. Stech, E. Stephenson, P. Tischhauser, and M. Wiescher, Nucl. Phys. A **654**, 924c (1999).
[10] J. Fisker, F.-K. Thielemann, and M. Wiescher, Astrophys. J. **608**, L61 (2004).
[11] A. Matic, A. M. van den Berg, M. N. Harakeh, H. J. Wörtche, G. P. A. Berg, M. Couder, J. L. Fisker, J. Görres, P. LeBlanc, S. O'Brien, M. Wiescher, K. Fujita, K. Hatanaka, Y. Sakemi, Y. Shimizu, Y. Tameshige, A. Tamii, M. Yosoi, T. Adachi, Y. Fujita, Y. Shimbara, H. Fujita, T. Wakasa, P. O. Hess, B. A. Brown, and H. Schatz, Phys. Rev. C **80**, 055804 (2009).
[12] A. Matic, A. M. van den Berg, M. N. Harakeh, H. J. Wörtche, G. P. A. Berg, M. Couder, J. Görres, P. LeBlanc, S. O'Brien, M. Wiescher, K. Fujita, K. Hatanaka, Y. Sakemi, Y. Shimizu, Y. Tameshige, A. Tamii, M. Yosoi, T. Adachi, Y. Fujita, Y. Shimbara, H. Fujita, T. Wakasa, B. A. Brown, and H. Schatz, Phys. Rev. C **82**, 025807 (2010).
[13] A. Matic, A. M. van den Berg, M. N. Harakeh, H. J. Wörtche, M. Beard, G. P. A. Berg, J. Görres, P. LeBlanc, S. O'Brien, M. Wiescher, K. Fujita, K. Hatanaka, Y. Sakemi, Y. Shimizu,

Y. Tameshige, A. Tamii, M. Yosoi, T. Adachi, Y. Fujita, Y. Shimbara, H. Fujita, T. Wakasa, J. P. Greene, R. Crowter, and H. Schatz, Phys. Rev. C **84**, 025801 (2011).

[14] S. Almaraz-Calderon, W. P. Tan, A. Aprahamian, M. Beard, G. P. A. Berg, B. Bucher, M. Couder, J. Görres, S. O'Brien, D. Patel, A. Roberts, K. Sault, M. Wiescher, C. R. Brune, T. N. Massey, K. Fujita, K. Hatanaka, D. Ishiwaka, H. Matsubara, H. Okamura, H. J. Ong, Y. Sakemi, Y. Shimizu, T. Suzuki, Y. Tameshige, A. Tamii, J. Zenihiro, T. Kubo, Y. Namiki, Y. Ohkuma, Y. Shimbara, S. Suzuki, R. Watanabe, R. Yamada, T. Adachi, Y. Fujita, H. Fujita, M. Dozono, and T. Wakasa, Phys. Rev. C **86**, 065805 (2012).

[15] C. M. Deibel, K. E. Rehm, J. M. Figueira, J. P. Greene, C. L. Jiang, B. P. Kay, H. Y. Lee, J. C. Lighthall, S. T. Marley, R. C. Pardo, N. Patel, M. Paul, C. Ugalde, A. Woodard, A. H. Wuosmaa, and G. Zinkann, Phys. Rev. C **84**, 045802 (2011).

[16] W. Hauser and H. Feshbach, Phys. Rev. **87**, 366 (1952).

[17] T. Rauscher, F.-K. Thielemann, and K. L. Kratz, Phys. Rev. C **56**, 1613 (1997).

[18] M. Wang, G. Audi, A. Wapstra, F. Kondev, M. MacCormick, X. Xu, and B. Pfeiffer, Chin. Phys. C **36**, 1603 (2012).

[19] C. Iliadis, *Nuclear Physics of Stars*, 2nd ed. (Wiley, New York, 2015).

[20] R. Paddock, Phys. Rev. C **5**, 485 (1972).

[21] S. Kubono, S. Kato, M. Yasue, H. Ohnuma, M. Sasao, K. Tsukamoto, and R. Kuramasu, Nucl. Phys. A **276**, 201 (1977).

[22] W. Alford, P. Craig, D. Lind, R. Raymond, J. Ullman, C. Zafiratos, and B. Wildenthal, Nucl. Phys. A **457**, 317 (1986).

[23] R. Neveling, H. Fujita, F. D. Smit, T. Adachi, G. P. A. Berg, E. Z. Buthelezi, J. Carter, J. L. Conradie, M. Couder, R. W. Fearick, S. V. Förtsch, D. T. Fourie, Y. Fujita, J. Görres, K. Hatanaka, M. Jingo, A. M. Krumbholz, C. O. Kureba, J. P. Mira, S. H. T. Murray, P. von Neumann-Cosel, S. O'Brien, P. Papka, I. Poltoratska, A. Richter, E. Sideras-Haddad, J. A. Swartz, A. Tamii, I. T. Usman, and J. J. van Zyl, Nucl. Instrum. Methods Phys. Res., Sect. A **654**, 29 (2011).

[24] Y. Fujita, K. Hatanaka, G. P. A. Berg, K. Hosono, N. Matsuoka, S. Morinobu, T. Noro, M. Sato, K. Tamura, and H. Ueno, Nucl. Instrum. Methods Phys. Res., Sect. B **126**, 274 (1997).

[25] H. Fujita, Y. Fujita, G. P. A. Berg, A. Bacher, C. Foster, K. Hara, K. Hatanaka, T. Kawabata, T. Noro, H. Sakaguchi, Y. Shimbara, T. Shinada, E. Stephenson, H. Ueno, and M. Yosoi, Nucl. Instrum. Methods Phys. Res., Sect. A **484**, 17 (2002).

[26] V. E. Iacob, J. C. Hardy, J. F. Brinkley, C. A. Gagliardi, V. E. Mayes, N. Nica, M. Sanchez-Vega, G. Tabacaru, L. Trache, and R. E. Tribble, Phys. Rev. C **74**, 055502 (2006).

[27] T. Tanabe, K. Haga, M. Yasue, K. Sato, K. Ogino, Y. Kadota, M. Tochi, K. Makino, T. Kitahara, and T. Shiba, Nucl. Phys. A **399**, 241 (1983).

[28] C. E. Rolfs and W. S. Rodney, *Cauldrons in the Cosmos: Nuclear Astrophysics* (University of Chicago Press, Chicago, 1988), p. 561.

[29] W. A. Richter, S. Mkhize, and B. A. Brown, Phys. Rev. C **78**, 064302 (2008).

[30] E. K. Warburton and B. A. Brown, Phys. Rev. C **46**, 923 (1992).

[31] S. M. Brown, W. N. Catford, J. S. Thomas, B. Fernández-Domínguez, N. A. Orr, M. Labiche, M. Rejmund, N. L. Achouri, H. Al Falou, N. I. Ashwood, D. Beaumel, Y. Blumenfeld, B. A. Brown, R. Chapman, M. Chartier, N. Curtis, G. De France, N. De Sereville, F. Delaunay, A. Drouart, C. Force, S. Franchoo, J. Guillot, P. Haigh, F. Hammache, V. Lapoux, R. C. Lemmon, A. Leprince, F. Maréchal, X. Mougeot, B. Mouginot, L. Nalpas, A. Navin, N. P. Patterson, B. Pietras, E. C. Pollacco, A. Ramus, J. A. Scarpaci, I. Stefan, and G. L. Wilson, Phys. Rev. C **85**, 011302(R) (2012).

[32] A. Gilbert and A. G. W. Cameron, Can. J. Phys. **43**, 1446 (1965).

[33] A. J. Koning, S. Hilaire, and M. C. Duijvestijn, AIP Conf. Proc. **769**, 1154 (2005).

[34] A. Koning, S. Hilaire, and S. Goriely, TALYS-1.8 User Manual, 2015.

[35] T. A. Carey, P. G. Roos, N. S. Chant, A. Nadasen, and H. L. Chen, Phys. Rev. C **29**, 1273 (1984).

[36] T. A. Carey, P. G. Roos, N. S. Chant, A. Nadasen, and H. L. Chen, Phys. Rev. C **23**, 576 (1981).

[37] N. Anantaraman, C. L. Bennett, J. P. Draayer, H. W. Fulbright, H. E. Gove, and J. Tke, Phys. Rev. Lett. **35**, 1131 (1975).

[38] T. Yamaya, M. Saitoh, M. Fujiwara, T. Itahashi, K. Katori, T. Suehiro, S. Kato, S. Hatori, and S. Ohkubo, Nucl. Phys. A **573**, 154 (1994).

[39] A. Volya and Y. M. Tchuvil'sky, Phys. Rev. C **91**, 044319 (2015).

[40] W. H. Press, S. A. Teukolsky, W. T. Vetterling, and B. P. Flannery, *Numerical Recipes in C* (Cambridge University Press, New York, 1992).

[41] P. D. Kunz and E. Rost, *Zero Range Distorted Wave Born Approximation* (Springer, Berlin, 1984).

[42] C. Iliadis, Nucl. Phys. A **618**, 166 (1997).

[43] P. Mohr, Phys. Rev. C **61**, 045802 (2000).

[44] T. Rauscher and F.-K. Thielemann, At. Data Nucl. Data Tables **75**, 1 (2000).